IIETA International Information and Engineering Technology Association
Advancing the World of Information and Engineering

Annales de Chimie - Science des Matériaux
Vol. 50, No. 1, February, 2026, pp. 65-72
Journal homepage: http://iieta.org/journals/acsm

Compressive Strength and Crack Patterns of 15 cm K-200 Concrete Cylinders

Hadi Kusnanto[1,2], Waluyo Adi Siswanto[2*], Supriyono[3], Mohammad Sukri Mustapa[4]

[1] Department of Mechanical Engineering, Universitas Muhammadiyah Surabaya, Surabaya 60113, Indonesia
[2] Postgraduate Mechanical Engineering, Manufacturing and Process Technology Research Group, Universitas Muhammadiyah Surakarta, Surakarta 57169, Indonesia
[3] Postgraduate Mechanical Engineering, Advanced Vehicle Control and Automation Research Group, Universitas Muhammadiyah Surakarta, Surakarta 57169, Indonesia
[4] Faculty of Mechanical and Manufacturing Engineering, Universiti Tun Hussein Onn Malaysia, Batu Pahat 86400, Malaysia

Corresponding Author Email: was123@ums.ac.id

Copyright: ©2026 The authors. This article is published by IIETA and is licensed under the CC BY 4.0 license (http://creativecommons.org/licenses/by/4.0/).

https://doi.org/10.18280/acsm.500107

Received: 1 December 2025
Revised: 12 February 2026
Accepted: 23 February 2026
Available online: 28 February 2026

Keywords:
concrete, concrete fracture, compression test, force distribution, concrete crack pattern

ABSTRACT

Understanding crack behavior in concrete under compression is essential for evaluating failure mechanisms and structural performance. This study investigates K-200 concrete cylinders (150 mm × 300 mm) tested at curing ages of 7, 14, and 28 days. A total of 24 specimens were examined, with compressive strengths ranging from 15.06 MPa at 14 days to 27.61 MPa at 7 days, and maximum applied forces between 205 kN and 332 kN. Crack development was strongly influenced by curing age, aggregate size, and press plate geometry. At 7 days, columnar swelling and cone failures were predominant, while splitting cracks appeared under flat plate loading. At 14 days, mixed cone–shear and cone–split failures emerged, indicating the interaction of compressive and tensile stresses. By 28 days, cone cracks became the prevailing mode, with shear cracks appearing in selected configurations. These findings underscore that compressive strength values alone do not fully describe concrete performance; the evolution of crack patterns provides critical insight into structural reliability and failure modes under axial loading.

1. INTRODUCTION

Cracks in concrete typically initiate at its weakest points, such as the interfacial transition zone (ITZ) between the aggregate and the cement paste [1, 2]. The inherent heterogeneity of concrete contributes to randomness of crack initiation and propagation [3, 4]. Under axial compression, cracks often originate from the ITZ and coarse aggregates, with their distribution and size influenced by the water–cement ratio [1]. Applied forces may generate diverse crack patterns depending on the loading conditions and the material properties of the concrete [5, 6]. Fracture mechanics examines crack propagation in materials under various loading conditions. The three principal fracture modes are Mode I, Mode II, and Mode III, each characterized by the application of stress and different crack propagation behaviors [7-11]. Increased surface roughness reduces the effective contact area and raises local pressure, affecting contact mechanics and pressure distribution [12-15]. Pressure Fluctuations Roughness-induced pressure fluctuations elevate maximum stress levels [15-17]. In addition, rough surfaces can increase contact temperature and reduce the load-carrying capacity [16, 18].

This article provides variables related to observed crack patterns, including test duration (s), maximum compressive force (kN), maximum stress (kg/cm²), and compressive strength (MPa). Crack patterns are documented across concrete age groups of 7, 14, and 28 days.

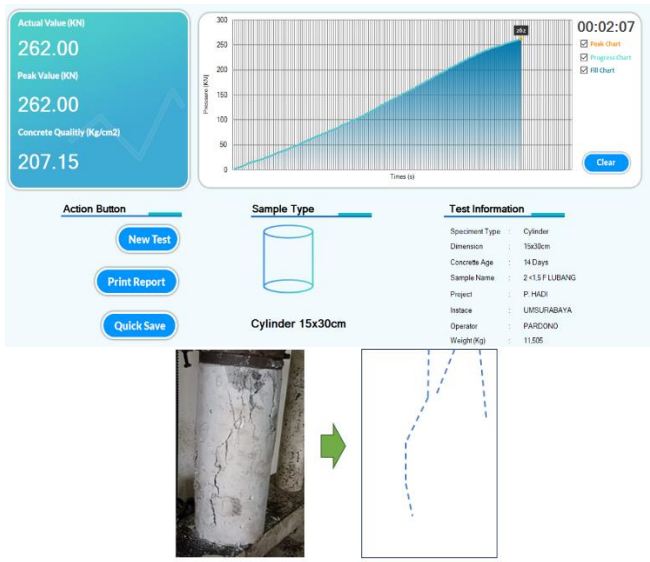

Figure 1. Typical compression test data and crack pattern model

The specimens consisted of cylindrical K-200 grade concrete with a diameter of 15 cm, designed to withstand loads

up to 200 kg/cm² in accordance with SNI 03-2834-2000 [19]. The experimental results presented in this study are intended to provide as input for numerical simulation models of crack behavior under compressive loadings. Figure 1 illustrates a representative example of the test results.

Recent publications have emphasized the importance of experimental results for validating numerical models and supporting reproducibility in concrete research. For example, collections of compressive strength data of concrete have been shared to aid predictive modelling and benchmarking [20, 21].

2. LIMITATIONS

The experimental results comprise a limited number of concrete compression tests conducted at three curing ages: 7 days, 14 days, and 28 days. Each age group included four specimens, resulting in a total of twelve compressive strength evaluations. The testing procedure follows the standards outlined in SNI 1974:2011 [22] and ASTM C39/C39M [23], which specify methods for determining the compressive strength of cylindrical concrete specimens. These standards ensured consistency in specimen preparation, loading conditions, and data acquisition throughout the testing process.

3. MATERIALS DESIGN

3.1 Concrete mix

The specimens were prepared using groundwater, Portland cement Type I, sand (density 2437–2536 kg/m³), and crushed stone (density 2594–2699 kg/m³). This mix composition was applied consistently across all cylindrical specimens.

3.2 Pressing material

The press plates were fabricated from mild steel with an ultimate tensile strength (UTS) of 350–620 MPa, providing sufficient resistance to applied loads during testing.

3.3 Testing machine

A locally manufactured compression testing machine (MBT brand) with a maximum capacity of 100,000 kN was used to conduct the compressive strength tests.

3.4 Capping material

Sulfur powder was used as the capping material, melted at a temperature of approximately 129 ℃ and applied in accordance with SNI 6369:2008 [24].

4. EXPERIMENTAL DESIGN AND METHODS

4.1 Materials and mix design

The concrete specimens were prepared in accordance with the SNI 03-2834-2000 standard [19]. The mix composition for each cylindrical specimen (150 mm diameter × 300 mm height) consisted of: water = 1.14 L, cement = 1.87 kg, sand = 3.87 kg, and crushed stone = 5.49 kg. This standardized mix ensured consistency across all test specimens.

4.2 Loading configuration

To vary the force distribution during compressive testing, two press models were fabricated from 15 mm thick steel plates with a diameter of 150 mm. One press plate contained a central hole, while the other was solid without a hole, as illustrated in Figure 2. These configurations were designed to investigate the influence of press geometry on crack initiation and propagation.

4.3 Specimen conditioning

Prior to testing, the concrete specimens were conditioned through wet curing by soaking, in accordance with SNI 2847:2013 [25] and SNI 2493:2011 [26]. Specimens tested at 7 days were soaked for 3 days, those tested at 14 days for 7 days, and those tested at 28 days also for 7 days. This curing procedure ensured proper hydration and strength development before testing.

The flow of the experimental procedure and data acquisition method is described in Figure 3.

Figure 3 illustrates the integrated system and workflow used for concrete compression testing and data acquisition. The testing procedure adheres to the standards outlined in SNI 1974:2011 [22] and ASTM C39/C39M [23], which specify the method for evaluating the compressive strength of cylindrical concrete specimens. The compressive force was applied through a hydraulic system, and the resulting output is measured by a transducer. This analog signal is amplified and converted into a digital format, then transmitted to a computer for real-time processing and visualization. The interface displayed both numerical data and graphical outputs, including compressive force curves and strength values.

The compression tests were conducted under load-controlled conditions to ensure a stable and gradual increase in compressive stress. The loading rate was controlled at approximately 0.20-0.30 MPa/s, allowing sufficient time for crack initiation and propagation to occur during the loading process [22, 23]. This controlled loading condition enabled clearer observation of crack patterns and failure modes in the concrete cylinders.

The results generated from this system includes duration (in seconds), maximum compressive force (in kN), and compressive strength values (in MPa), all recorded in accordance with the block diagram shown in Figure 3. These figures are visible on the computer screen and can be printed directly from the compression testing machine. In addition to numerical data, visual documentation of the testing process was captured using a 1.2-megapixel resolution camera, providing supplementary photo and video records of specimen behavior during loading. This integrated approach ensures traceability, enhances data reliability, and supports both quantitative and qualitative analysis of concrete performance under compressive stress.

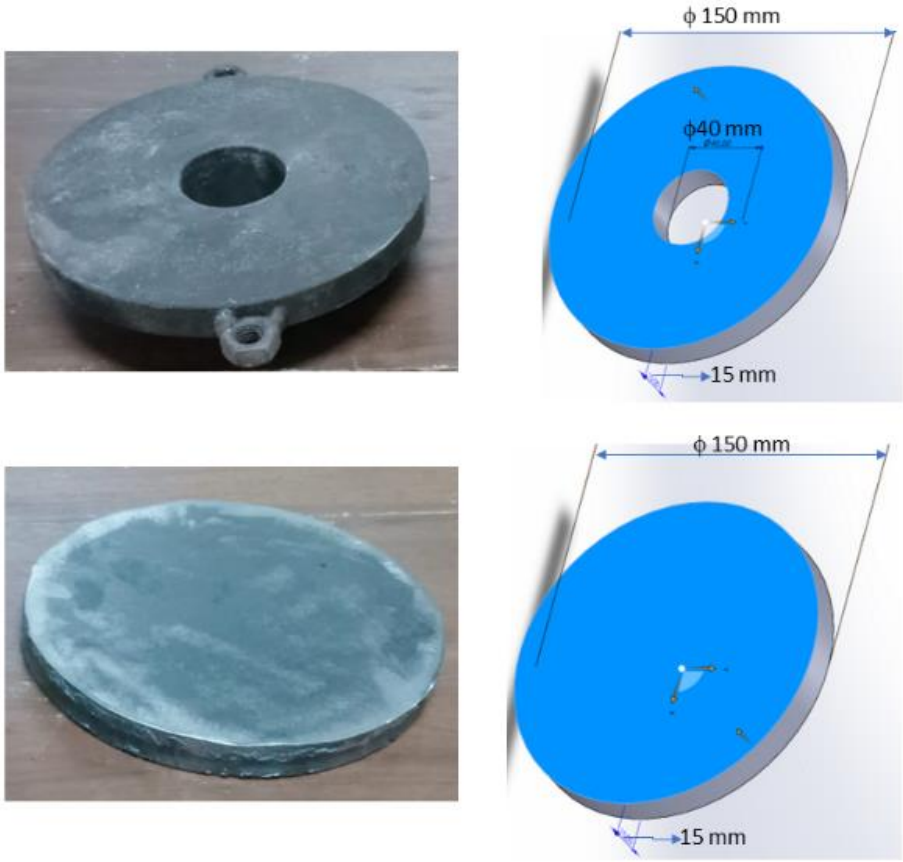

Figure 2. Pressing materials used in compressive testing, consisting of steel plates: flange with hole (FH) and flat flange (FF) configurations

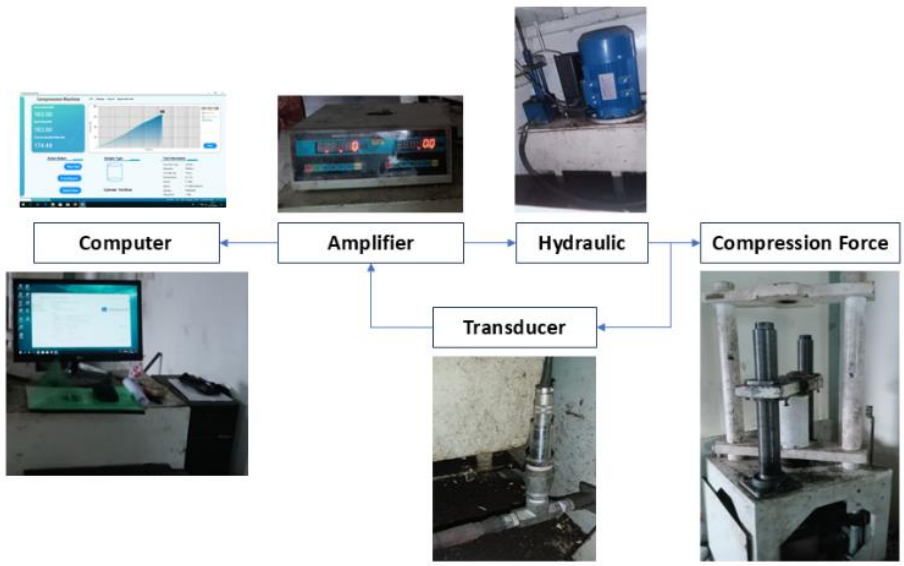

Figure 3. Schematic flow of testing and data acquisition system for concrete compression experiments

5. DATA DESCRIPTION

The test results were organized into three groups based on concrete age: 7, 14, and 28 days. They include both numerical and graphical outputs derived from compression testing. Results were systematically tabulated by age group and specimen weight (kg), loading duration (s), maximum compressive force (kN), and compressive strength expressed in MPa and kg/cm².

5.1 Compressive strength test results

5.1.1 Test results of concrete at ages 7 days

The compressive testing results for 7-day-old concrete specimens were grouped by aggregate size: ≤ 1.5 cm and > 1.5 cm. The recorded values, including maximum compressive force (kN) and corresponding compressive strength (MPa) are summarized in Table 1.

Table 1. Compressive strength of concrete at 7 days

Code Sample	Specimen Mass (kg)	Duration (s)	Max Force (KN)	Concrete Qty	
				kg/cm²	MPa
1.5-FH₁-01	11.62	173	205	219.44	17.86
1.5-FH₂-02	11.665	178	225	241.2	19.62
1.5+FH₁-03	12.035	122	248	265.47	21.6
1.5+FH₂-04	12.035	183	292	312.56	25.43
1.5-FF₁-05	11.91	138	213	228	18.55
1.5-FF₂-06	11.66	110	258	276.17	22.47
1.5+FF₁-07	12.045	201	317	339.32	27.61
1.5+FF₂-08	12.095	142	239	255.83	20.82

Table 2. Compressive strength of concrete at 14 days

Code Sample	Specimen Mass (kg)	Duration (s)	Max Force (KN)	Concrete Qty	
				kg/cm²	MPa
1.5-FH₁-09	11.705	93	234	185.01	15.06
1.5-FH₂-10	11.505	127	262	207.15	16.86
1.5+FH₁-11	11.67	142	256	202.41	16.47
1.5+FH₂-12	11.89	112	292	230.87	18.79
1.5-FF₁-13	11.725	129	319	252.22	20.52
1.5-FF₂-14	11.375	102	271	214.79	17.48
1.5+FF₁-15	11.76	129	303	239.57	19.49
1.5+FF₂-16	11.725	121	285	224.28	18.25

Table 3. Compressive strength of concrete at 28 days

Code Sample	Specimen Mass (kg)	Duration (s)	Max Force (KN)	Concrete Qty	
				kg/cm²	MPa
1.5-FH₁-17	11.6	118	329	228.91	18.63
1.5-FH₂-18	11.59	106	292	203.17	16.53
1.5+FH₁-19	12.03	97	329	228.91	18.63
1.5+FH₂-20	12.028	81	332	231	18.8
1.5-FF₁-21	11.6	118	329	228.91	18.63
1.5-FF₂-22	11.59	106	292	203.17	16.53
1.5+FF₁-23	12.035	113	309	215	17.49
1.5+FF₂-24	12.032	82	317	220.56	17.95

Representative results for each aggregate group are shown in Figures 4 and 5.

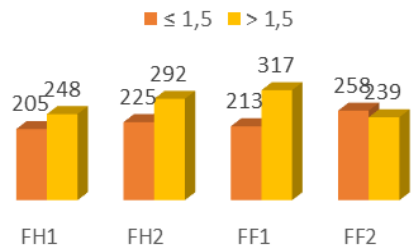

Figure 4. Maximum compressive force (kN) in 7-day-old concrete specimens: flange with hole (FH) and flat flange (FF) suppressor

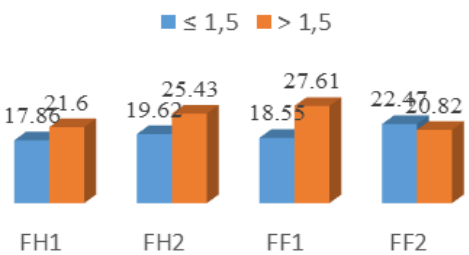

Figure 5. Compressive strength values (MPa) of 7-day-old concrete specimens: flange with hole (FH) and flat flange (FF) suppressor

5.1.2 Test results of concrete at ages 14 days

The summary of test data for 14-day-old concrete is in Table 2. Figures 6 and 7 present the compressive testing results of 14-day-old concrete specimens under two different suppressor conditions: flange with hole (FH) and flat flange (FF).

Figure 6 illustrates the maximum compressive force (kN) recorded during testing, while Figure 7 shows the corresponding compressive strength values (MPa). Together, these figures provide a comparative view of the mechanical performance of concrete at 14 days of age, highlighting the influence of suppressor type on both the applied force and the resulting strength.

The combined graphical outputs complement the tabulated test results by linking numerical values with visual representation, thereby facilitating analysis of specimen behavior under compressive loading.

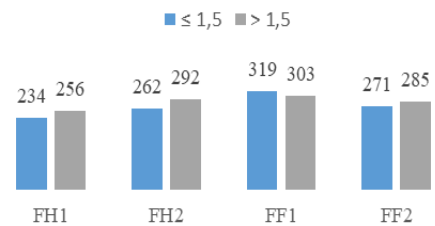

Figure 6. Maximum compressive force (kN) in 14-day-old concrete: flange with hole (FH) and flat flange (FF) suppressor

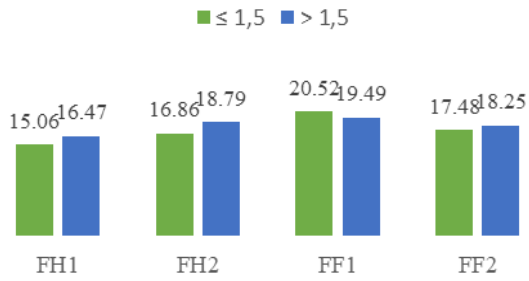

Figure 7. Compressive strength value (MPa) for concrete in 14-day-old: flange with hole (FH) and flat flange (FF) suppressor

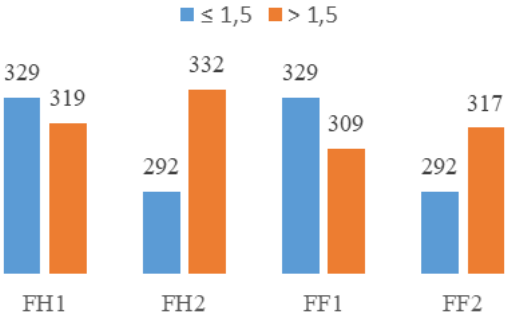

Figure 8. Maximum compressive force (kN) at 28-day-old concrete: flange with hole (FH) and with flat flange (FF) suppressor

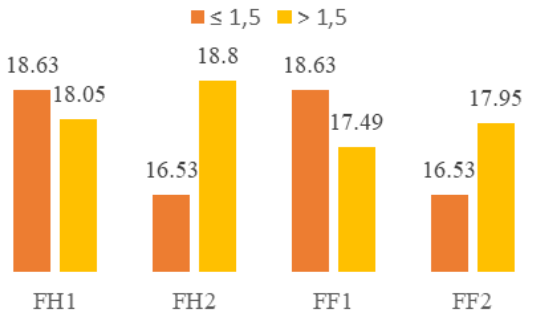

Figure 9. Compressive strength value (MPa) for concrete aged 28 days: flange with hole (FH) and flat flange (FF) suppressor

5.1.3 Compressive strength of concrete at 28 days

The summary of test data for 28-day-old concrete is in Table 3. Figures 8 and 9 present the compressive testing results of 28-day-old concrete specimens under two suppressor conditions: FH and FF.

Figure 8 shows the maximum compressive force (kN) recorded during testing, while Figure 9 presents the corresponding compressive strength values (MPa). Together, these figures compare the mechanical performance of 28 days concrete, highlighting the influence of suppressor type on applied force and resulting strength. The graphical outputs complement the tabulated data by linking numerical values with visual documentation, enabling deeper analysis of specimen behavior under compressive loading.

5.2 Crack patterns

5.2.1 Crack patterns of concrete at 7 days

Figures 10 and 11 show the crack patterns observed in 7-day-old concrete specimens subjected to compressive testing under two different loading conditions. Figure 10 presents the crack formation in specimens tested using an FH, while Figure 11 presents the crack pattern in specimens tested with a punch without holes (FF). These visual records complement the numerical data by documenting the fracture behavior of the concrete at an early age. Together, the figures provide qualitative evidence of how different press configurations influence crack initiation and propagation, offering a visual counterpart to the mechanical performance data reported in the preceding tables and figures. The classification of crack patterns in 7-day-old concrete specimens is summarized in Table 4.

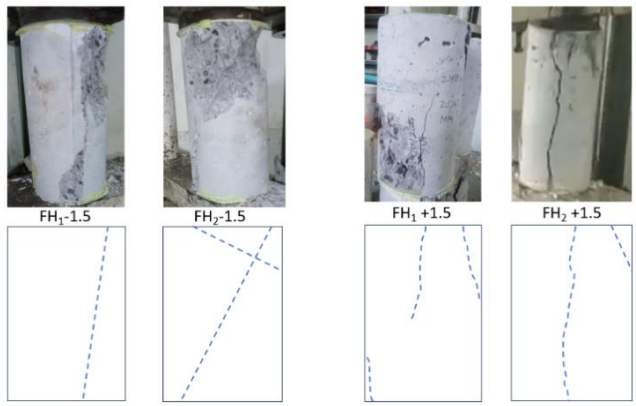

Figure 10. Crack pattern in 7-day-old concrete tested with flange with hole (FH) suppressor

Table 4. Classification of crack models in 7-day-old concrete

Code Sample	Crack Type	Crack Shape	Main Cause
1.5-FH$_1$-01	Columnar	Swelling without obvious cracks	High friction between the test machine plate and the specimen
1.5-FH$_2$-02	Cone and shear	Combination of cone and diagonal	Normal failure mode
1.5+FH$_1$-03	Columnar	Swelling without obvious cracks	High friction between the test machine plate and the specimen
1.5+FH$_2$-04	Columnar	Swelling without obvious cracks	High friction between the test machine plate and the specimen
1.5-FF$_1$-05	Columnar	Swelling without obvious cracks	High friction between the test machine plate and the specimen
1.5-FF$_2$-06	Columnar	Swelling without obvious cracks	High friction between the test machine plate and the specimen
1.5+FF$_1$-07	Cone	Cone at the tip	Compression and shear stress
1.5+FF$_2$-08	Splitting	Vertical crack	Lateral tensile stress

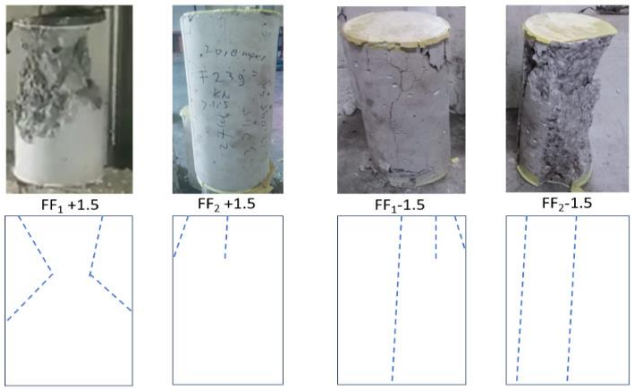

Figure 11. Crack pattern in 7-day-old concrete tested with flat flange (FF) suppressor

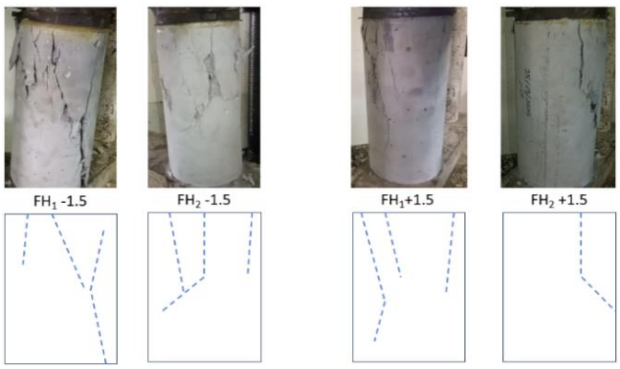

Figure 12. Crack pattern in 14-day-old concrete tested with flange with hole (FH) suppressor

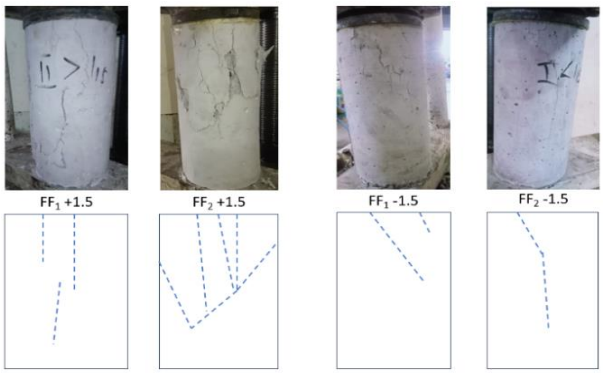

Figure 13. Crack pattern in 14-day-old concrete tested with flat flange (FF) suppressor

5.2.2 Crack patterns of concrete at ages 14 days

Figures 12 and 13 show the crack patterns observed in 14-day-old concrete specimens subjected to compressive testing under two different loading conditions. Figure 12 presents the crack formation in specimens tested using a hole press (FH), while Figure 13 presents the crack pattern in specimens tested with a punch without holes (FF). These visual records complement the mechanical data by documenting fracture behavior at the intermediate curing stage, providing qualitative evidence of crack initiation and propagation under different press configurations. The classification of crack patterns in 14-day-old concrete tests is summarized in Table 5.

5.2.3 Crack patterns of concrete at ages 28 days

Figures 14 and 15 show the crack patterns observed in 28-day-old concrete specimens under compressive loading. Figure 14 presents cracks in specimens tested with a hole press (FH), whereas Figure 15 shows cracks in specimens tested with a punch without holes (FF). Together, these figures provide visual documentation of fracture behavior in mature concrete, linking crack propagation to the mechanical performance data reported for this age group. The classification of crack patterns in 28-day-old specimens is summarized in Table 6.

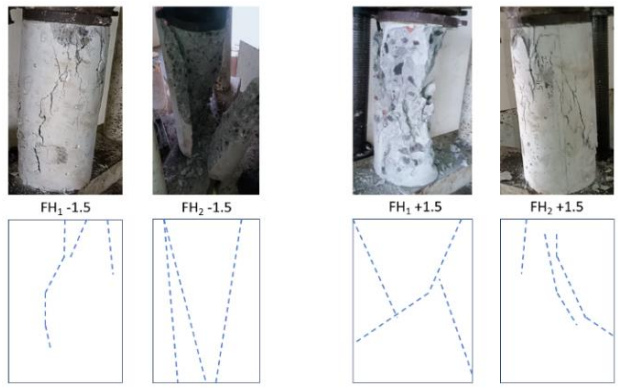

Figure 14. Crack pattern in 28-day-old concrete tested with flange with hole (FH) suppressor

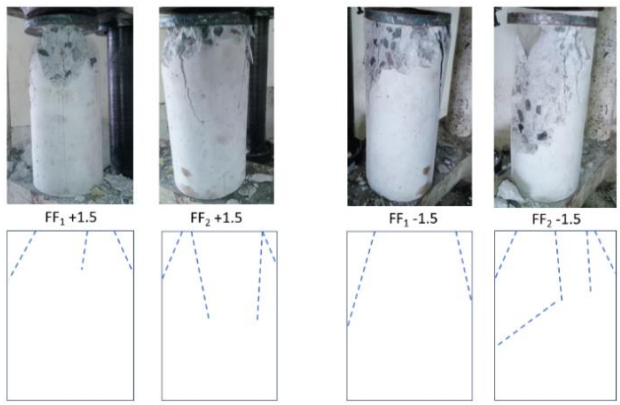

Figure 15. Crack pattern in 28-day-old concrete tested with flat flange (FF) suppressor

Table 5. Classification of crack models in 14-day-old concrete

Code Sample	Crack Type	Crack Shape	Main Cause
1.5-FH_1-09	Cone and shear	Combination of cone and diagonal	Normal failure mode
1.5-FH_2-10	Cone and split	combination of vertical crack and conical at the tip	Combination of compressive, shear, and lateral tensile stress
1.5+FH_1-11	Cone	Cone at the tip	Compression and shear stress
1.5+FH_2-12	Cone and split	combination of vertical crack and conical at the tip	Combination of compressive, shear, and lateral tensile stress

1.5-FF_1-13	Shear	Diagonal crack	Shear stress
1.5-FF_2-14	Cone and split	combination of vertical crack and conical at the tip	Combination of compressive, shear, and lateral tensile stress
1.5+FF_1-15	Columnar	Swelling without obvious cracks	High friction between the test machine plate and the specimen
1.5+FF_2-16	Cone and Split	combination of vertical crack and conical at the tip	Combination of compressive, shear, and lateral tensile stress

Table 6. Classification of crack models in 28-day-old concrete

Code Sample	Crack Type	Crack Shape	Main Cause
1.5-FH_1-17	Columnar	Swelling without obvious cracks	High friction between the test machine plate and the specimen
1.5-FH_2-18	Columnar	Swelling without obvious cracks	High friction between the test machine plate and the specimen
1.5+FH_1-19	Cone	Cone at the tip	Compression and shear stress
1.5+FH_2-20	Shear	Diagonal crack	Shear stress
1.5-FF_1-21	Cone	Cone at the tip	Compression and shear stress
1.5-FF_2-22	Cone	Cone at the tip	Compression and shear stress
1.5+FF_1-23	Cone	Cone at the tip	Compression and shear stress
1.5+FF_2-24	Cone	Cone at the tip	Compression and shear stress

6. CONCLUSIONS

This study systematically investigated the compressive strength and crack patterns of K-200 concrete cylinders at curing ages of 7, 14, and 28 days, under varying aggregate sizes and press plate geometries. The results demonstrate that compressive strength alone does not fully capture the mechanical performance of concrete; the evolution of crack patterns provides critical insight into failure mechanisms and structural reliability.

Crack development is strongly influenced by curing age, aggregate size, and press plate configuration. Early-age specimens (7 days) exhibited columnar swelling and cone failures, while intermediate specimens (14 days) showed mixed cone–shear and cone–split modes. Mature specimens (28 days) were dominated by cone cracks, with shear cracks appearing in selected configurations.

Comparative analysis across aggregate groups revealed measurable variations in maximum compressive force and strength values, confirming the role of material heterogeneity in fracture behavior.

The experimental results, obtained through standardized procedures (SNI and ASTM), provide a reliable dataset for both experimental and numerical research. These findings can serve as validated input for simulation models of crack behavior under compressive loads, supporting more accurate benchmarking and predictive modeling. The integration of numerical data with visual documentation further enhances reproducibility and facilitates comparative studies across diverse research contexts.

Overall, this study contributes to a deeper understanding of concrete fracture mechanics, with practical relevance for structural engineering, construction quality assessment, and the development of analytical methods for modeling crack behavior under compression

ACKNOWLEDGMENT

The authors gratefully acknowledge the financial support provided by the Ministry of Higher Education, Science, and Technology of Indonesia through the Doctoral Dissertation Research Grant scheme (Grant No. 007/LL6/PL/AL.04/2025; 168.68/A.3-III/LRI/VI/2025).

REFERENCES

[1] Huang, Y.J., He, X.J., Wang, Q., Xiao, J.Z. (2019). Deformation field and crack analyses of concrete using digital image correlation method. Frontiers of Structural and Civil Engineering, 13: 1183-1199. https://doi.org/10.1007/s11709-019-0545-3

[2] Ramli, R., Azlan, A.A.N., Osman, S., Zakaria, M.N., Yahaya, S.M. (2025). Characterization of pineapple leaves reinforced cement based composites. In Proceedings of the Green Materials and Electronic Packaging Interconnect Technology Symposium, pp. 279-287. https://doi.org/10.1007/978-981-96-2871-1_40

[3] Zeng, M.H., Wu, Z.M., Wang, Y.J. (2020). A stochastic model considering heterogeneity and crack propagation in concrete. Construction and Building Materials, 254: 119289. https://doi.org/10.1016/j.conbuildmat.2020.119289

[4] Wang, J., Li, L., Zhang, X.G., Zhao, Y.G. (2020). A prediction model for concrete cracks due to chloride-induced corrosion. Advances in Materials Science and Engineering, 2020(1): 1049258. https://doi.org/10.1155/2020/1049258

[5] Srinivasan, S.S., Ferron, R.D. (2021). Effect of crack width, density, and depth on strength and durability of concrete equivalent mortar. ACI Materials Journal, 118(4): 65-77. https://doi.org/10.14359/51732792

[6] Koschemann, M., Curbach, M. (2024). Bond creep and its influence on crack width development. Bauingenieur, 99(11): 374-383. https://doi.org/10.37544/0005-6650-2024-11-60

[7] Deepa, A., Rajyalakshmi, G., Jayakrishna, K., Gowdaman, R. (2024). Structural integrity of laminates: Fracture modes I, II, and I/II under various loads. In Fracture Behavior of Nanocomposites and Reinforced Laminate Structures, pp. 111-122. https://doi.org/10.1007/978-3-031-68694-8_5

[8] Suárez, F., Felipe-Sesé, L., Castilla-Gonzalo, F.J., Díaz-Garrido, F. (2022). Study of the effect of fibre addition on mode II fracture of quasi-brittle materials. Dyna,

97(2): 195-202. https://doi.org/10.6036/10161
[9] Zhao, Y., Zheng, K., Wang, C.L. (2024). Rock Fracture Mechanics and Fracture Criteria. Springer Singapore. https://doi.org/10.1007/978-981-97-5822-7
[10] Poapongsakorn, P., Wiangkham, A., Aengchuan, P., Noraphaiphipaksa, N., Kanchanomai, C. (2020). Time-dependent fracture of epoxy resin under mixed-mode I/III loading. Theoretical and Applied Fracture Mechanics, 106: 102445. https://doi.org/10.1016/j.tafmec.2019.102445
[11] Wang, Y.L., Wang, W.G., Zhang, B.H., Li, C.Q. (2020). A review on mixed mode fracture of metals. Engineering Fracture Mechanics, 235: 107126. https://doi.org/10.1016/j.engfracmech.2020.107126
[12] Li, L., Yun, Q.Q., Tian, H.F., Cai, A.J., Cao, C.Y. (2019). Investigation into the contact characteristics of rough surfaces with surface tension. Journal of the Brazilian Society of Mechanical Sciences and Engineering, 41(8): 343. https://doi.org/10.1007/s40430-019-1847-z
[13] Olshevskiy, A., Yang, H.I., Kim, C.W. (2012). Finite element simulation of inelastic contact for arbitrarily shaped rough bodies. Proceedings of the Institution of Mechanical Engineers, Part C: Journal of Mechanical Engineering Science, 226(3): 595-606. https://doi.org/10.1177/0954406211417216
[14] Urzică, A.C., Bălan, M.R.D., Creţu, S.S. (2012). Pressures distributions and depth stresses developed in concentrated contacts between elements with non-Gaussian rough surfaces. In ASME 2012 11th Biennial Conference on Engineering Systems Design and Analysis, pp. 547-554. https://doi.org/10.1115/ESDA2012-82357
[15] Gao, C., Cai, L., Bi, Q.S. (2004). Micro-elastohydrodynamics lubrication of point contacts with coexistence of longitudinal and transverse roughness. International Journal of Nonlinear Sciences and Numerical Simulation, 5(2): 113-120. https://doi.org/10.1515/IJNSNS.2004.5.2.113
[16] Hooke, C.J. (2005). The effect of roughness in EHL contacts. Tribology and Interface Engineering Series, 48: 31-46. https://doi.org/10.1016/s0167-8922(05)80006-9
[17] Siswanto, W.A., Martama, B.P. (2019). Stress and deflection of a concrete block in a four-point bending (FPB) test. Universal Journal of Mechanical Engineering, 7(6): 307-317. https://doi.org/10.13189/ujme.2019.070601
[18] Chang, L.M., Jeng, Y.R. (2013). Effects of negative skewness of surface roughness on the contact and lubrication of nominally flat metallic surfaces. Proceedings of the Institution of Mechanical Engineers, Part J: Journal of Engineering Tribology, 227(6): 559-569. https://doi.org/10.1177/1350650112465365
[19] Badan Standar Nasional Indonesia. (2000). Tata cara pembuatan rencana campuran beton normal. https://repository.unikom.ac.id/64987/1/sni-03-2834-2000.pdf.
[20] Durrani, O., Haroon, A. (2026). Dataset on compressive strength, ultrasonic pulse velocity, and rebound hammer properties of ultra-high performance concrete with maturing age. Data in Brief, 64: 112267. https://doi.org/10.1016/j.dib.2025.112267
[21] Del Savio, A.A., Torres, A.L., Cárdenas-Salas, D., Olivera, M.V., Ibarra, G.U. (2025). Dataset for training neural networks in concrete crack detection: Laboratory-classified beam and column images. Data in Brief, 61: 111643. https://doi.org/10.1016/j.dib.2025.111643
[22] Badan Standar Nasional Indonesia. (2011). Cara uji kuat tekan beton dengan benda uji silinder. https://imsippoliban.wordpress.com/wp-content/uploads/2016/03/10532_1974_2011.pdf.
[23] ASTM C39/C39M. (2021). Standard test method for compressive strength of cylindrical concrete specimens 1.
[24] Badan Standardisasi Nasional Indonesia. (2008). Tata cara pembuatan kaping untuk benda uji silinder beton. SNI 6369:2008.
[25] Badan Standardisasi Nasional Indonesia. (2013). Persyaratan beton struktural untuk bangunan Gedung. SNI 2847:2013.
[26] Badan Standar Nasional Indonesia. (2011). Tata cara pembuatan dan perawatan benda uji beton di laboratorium. SNI 2493:2011.

APPENDIX

Experimental Data publicly available in Figshare Archive. https://doi.org/10.6084/m9.figshare.30647387.